Supporting Information

Pedraja et al. 10.1073/pnas.1712380115

Modeling the Fish in the Shuttle

To model the electric field arising from the complex geometry of a fish positioned within the Perspex shuttle, we used a finite-element modeling (FEM) approach. Fig. S3*A* shows the setup and resulting voltage map (see color bar) for a 21-cm fish (*Apteronotus*) (1) in a shuttle (conductivity 5×10^{-13} $\mu S \cdot cm^{-1}$) with an open slit (width 6 mm; water conductivity 230 $\mu S \cdot cm^{-1}$). The model fish is based on experimental data provided by B. Rasnow and C. Assad (1) and is 50% larger than the fish used in the present experiments. To ensure that signal contrast would not be overestimated due to the larger fish being effectively closer to the shuttle walls, the distance between the shuttle walls was scaled accordingly (i.e., walls were separated by 6 cm in the model compared with 4 cm in the behavioral setup, so that when centered, the model fish is 3 cm from each shuttle wall). Because electrical contrast is a key determinant of the EI, a slit (open to water or an aluminum stripe) on an insulating Perspex background produces an EI that is very similar to that of a conductive sphere or rod in water. Fig. S3*B* shows a comparison of the EIs of different cue types (metal slit, metal rod, open slit). Note that the EI profiles were very similar irrespective of the cue used. Also, the normalized EI profile is invariant to the width of the slit (Fig. S3*C*), just as that of a sphere is invariant to the radius (2). Finally, it is well known that as the lateral distance of a sphere decreases, the slope of the normalized EI increases while the width decreases (1–3). We find this is also the case for the shuttle with an open slit (Fig. S3*D*; compare with unnormalized data in Fig. 1 and Fig. S2).

Predicting the Magnitude of the Parallax-Induced Shift

We used the image–object ratio IOR (IOR = $\Delta_{image}/\Delta_{object}$; see main text) as determined from our BEM simulations (Fig. 1 *F–H*) to predict how much the fish would shift its position under the different speed conditions (i.e., right shuttle wall moving at 90% and 70% of the left wall speed). Fig. S4*A* shows IOR curves for the right (solid black line) and left (dotted black line) sides of the shuttle in *Gnathonemus*. It is important to note that the IOR will vary quantitatively with the translation range and specific position of an object within the electric field. The IOR curves shown here were calculated using a longitudinal object translation of 8 cm (i.e., the magnitude of the shuttle's movement in the behavioral experiments). For the reduced-speed conditions (70% and 90%), the right side of the shuttle translates across a reduced range of the fish's electric field compared with the 100% side. Thus, we recalculated the IOR curves accordingly (Fig. S4*A*, dark green: 90% object translation 7.2 cm; light green: 70%, 5.6 cm). Under the assumption that fish use electrosensory parallax, the point where the apparent speeds of left and right sides are the same predicts where the shuttle center position should be perceived. We calculated velocity balance curves from the left–right IOR differences (IORleft−IORright) scaled to a reference speed of 2 $cm \cdot s^{-1}$. Under control conditions (both sides move at 100%), this curve is zero (balanced) at position 0 (Fig. S4*B*, solid black line). If the right side moves more slowly, the velocity balance between left and right sides shifts upward by an amount proportional to the right–left speed difference (Fig. S4*B*, dark green: 90%; light green: 70%). Similarly, we calculated velocity balance curves for *Apteronotus* (Fig. S4*C*) and *Eigenmannia* (Fig. S4*D*). These curves were used to predict the magnitude of the animals' shift in our behavioral experiments, based on the notion that the centered position is perceived differently in the different speed conditions. As described in the main text, the predicted shifts match the trends observed in the behavioral data, including those reflected by interspecies differences (Fig. 2*C*, open circles vs. boxplots), but the amplitudes of the predictions were in general greater than those observed. This could reflect quantitative differences in electric fields, both in the models and individual variation among fish, among other things, but also suggests the presence of other, potentially competing perceptual cues (see main text and below).

A Simple Model of Centering Behavior

The discrepancy in shift amplitudes between our predictions and the actual behavioral response (Fig. 2*C*), as well as the fact that the distribution of fish positions increased in skewness rather than showing a translational shift under test conditions (Fig. 2*B*), suggests that in addition to a parallax cue (causing the fish to shift toward the slower side), there was also at least one other, competing cue (causing the fish to remain at the true center or move to the opposite side). Balancing EI amplitude on both sides of the body would be a potential candidate, as described in the main text.

As a first step toward understanding this multisensory decision process, we tested a simple dynamic model in which fish position was determined by two competing probabilistic factors. The primary dynamics of fish position $X(t)$ are described by a linear first-order system given by $\beta \dot{X}(t) = X_o - X(t)$, where β is a behavioral response time and X_o is a target position. In other words, fish position converges to X_o with a time constant β. The decision process is modeled by the choice of X_o. We assume that X_o is a random number drawn from one of two Gaussian distributions [$N_1(0,\sigma)$ or $N_2(\mu,\sigma)$] with a mean of 0 (indicating the centered position) or μ (indicating the parallax-predicted position), respectively. These distributions were modeled with the same SD σ because at this point we do not know the sensory precision of the parallax or any other conflicting cue. At fixed time intervals τ (that represent the sensory acquisition time), a new value of X_o is chosen with probability p from N_1 (indicating a decision to move toward a centered position); otherwise it is chosen from N_2 (indicating a decision to move toward a shifted position). The parameter μ was set to 0, 2.2, and 8.6 as predicted as the perceptual center for the different speed conditions of *Eigenmannia* (Fig. S4*D*). Although we do not present an exhaustive survey of the model, the $X(t)$ dynamics produce a bimodal or skewed distribution for a wide range of the free parameters (β, τ, σ, and p). Fig. S8 shows the position distribution obtained during behavioral experiments with *Eigenmannia* along with our model results.

1. Babineau D, Longtin A, Lewis JE (2006) Modeling the electric field of weakly electric fish. *J Exp Biol* 209:3636–3651.
2. Rasnow B (1996) The effects of simple objects on the electric field of *Apteronotus*. *J Comp Physiol A* 178:397–411.
3. Hofmann V, Sanguinetti-Scheck JI, Gómez-Sena L, Engelmann J (2013) From static electric images to electric flow: Towards dynamic perceptual cues in active electroreception. *J Physiol Paris* 107:95–106.

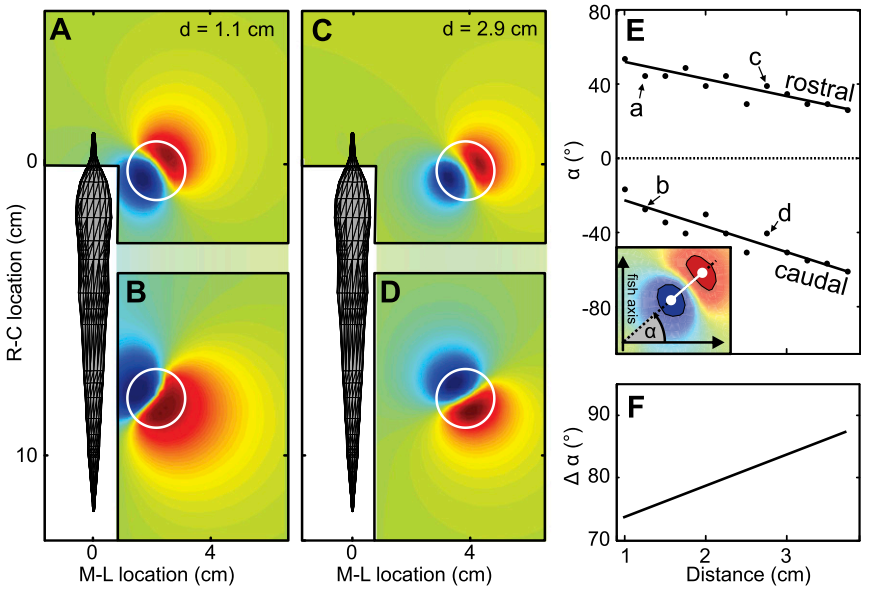

Fig. S1. The electric field geometry provides a basis for the electrosensory parallax cue. (*A*–*D*) Electric field perturbations due to a metal sphere (1-cm radius) positioned at different rostral–caudal locations and lateral distances (*A* and *B*, d = 1.1 cm; *C* and *D*, d = 2.9 cm). See also further explanations in the main text and Fig. 1. (*E*) The object polarization direction for rostral (*Upper* curve) and caudal (*Lower* curve) object positions at varying distances relative to the fish's rostral–caudal axis. The letters in the plot refer to points corresponding to the data shown in *A*–*D*. (*Inset*) Angle α was defined by the direction of the polarization gradient (white line) and the fish axis. Both for the rostral as well as for the caudal object location, the orientation angle (α) of this polarization systematically changes with increasing lateral distance. Linear fits to the model data are shown by the black lines. (*F*) The difference in the polarization direction between rostral and caudal positions (angle difference Δα) as a function of lateral distance. The angle difference increases linearly with increasing lateral distance (Movie S1) and reflects the dependency of the EI translation (Δ_{image}, Fig. 1) on lateral distance. As such, the electric field geometry and the resultant direction of object polarization are the physical bases of the electrosensory parallax cue.

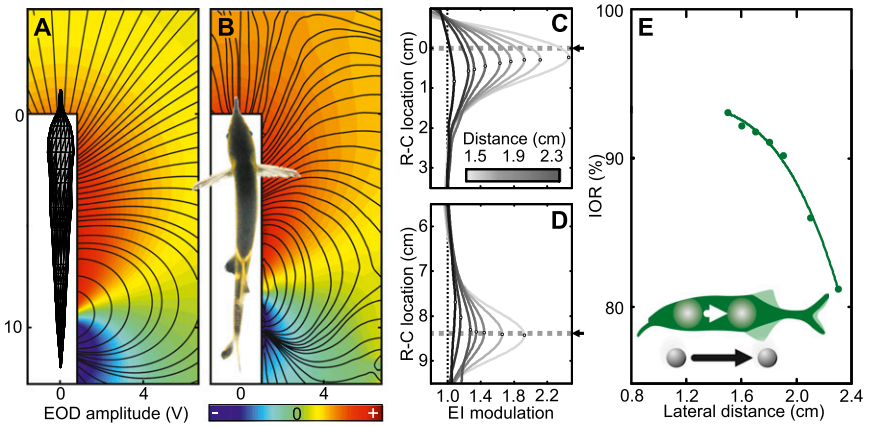

Fig. S2. Experimental validation of the model in *Gnathonemus petersii*. (*A* and *B*) *Top* view of the BEM-modeled (see also Fig. 1*A*) and experimentally measured basal electric fields of *G. petersii*. Voltage is shown as a color map (red, positive and blue, negative); black contour lines show the current flow (i.e., electric field). The white areas close to the fish comprise points where experimental measurements were not carried out. (*C* and *D*) Experimentally measured electric images (EI, see *Supporting Information* for details) of a metal sphere (1-cm radius) located at rostral (*C*) or caudal (*D*) locations along the body but at different lateral distances (1.5–2.3 cm; see gradient). The location of the object along the rostral–caudal axis of the animal is indicated by the gray dotted lines (*C*, 0 cm; *D*, 8.2 cm; location of the fish mouth was at 0 cm). Note that the amplitude of the EI decreases with increasing lateral distance, while the EI peak (open circles) shifts toward the midbody. (*E*) The image-to-object ratio (IOR) (see main text) for the two rostral–caudal object locations shown in *C* and *D*. The ratio decreases with increasing lateral distance, indicating that a more distant object would appear to be moving slower during relative motion. Solid line shows a power-law fit to the data; RMSE, 0.23%. (*Inset*) Sketch of fish illustrating the IOR, which is the ratio of the length of the white and the black arrows.

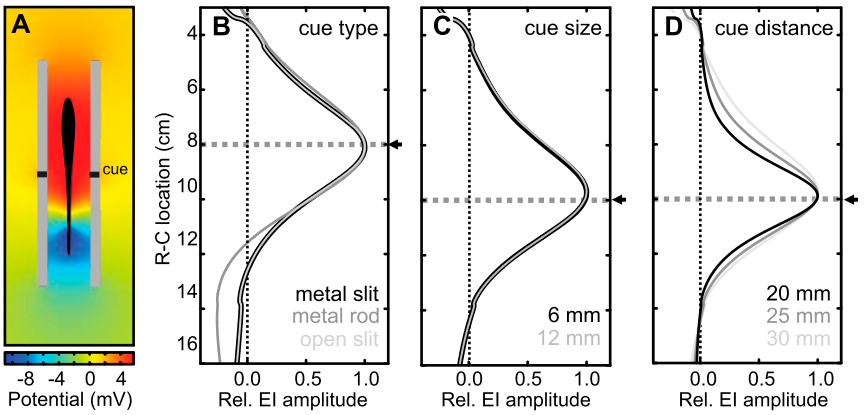

Fig. S3. FEM model of the electric field perturbed by the behavioral shuttle setup. (*A*) Voltage map for the fish in a shuttle with a 6-mm open slit. These results are based on the finite-element model described previously (1) and were used to compare electric images of the Perspex shuttle and a metal rod; see *Supporting Information* for more details. (*B*) Normalized (by peak value) electric images produced for different cue types (dark gray, metal rod with radius = 2.5 cm and metal conductivity 3.8×10^{11} μS·cm^{-1}; black, shuttle with metal-filled slit, width = 6 mm; and light gray, shuttle with open slit, width = 6 mm). Position of the electrosensory cue was 8-cm (gray dotted line, fish mouth was at 0 cm) and at 3-cm lateral distance. (*C*) Normalized electric images produced by different cue sizes (slit width). Cue was an open slit in the shuttle wall (black, 6 mm width; gray, 12 mm width) located at 10-cm (gray dotted line) and 3-cm lateral distance. (*D*) Normalized electric images produced by the cue at different distances. Cue was an open slit in the shuttle wall with a width of 6 mm located at 10 cm (gray dotted line) at varying distance (black, 20 mm; dark gray, 25 mm; and light gray, 30 mm). Similar to the EI parameters known for a sphere, the shuttle slit produced an EI that increased in relative slope with proximity (i.e., image width decreased and slope increased). Note that the 30-mm condition represents the EI a fish would experience when being centered in our behavioral apparatus.

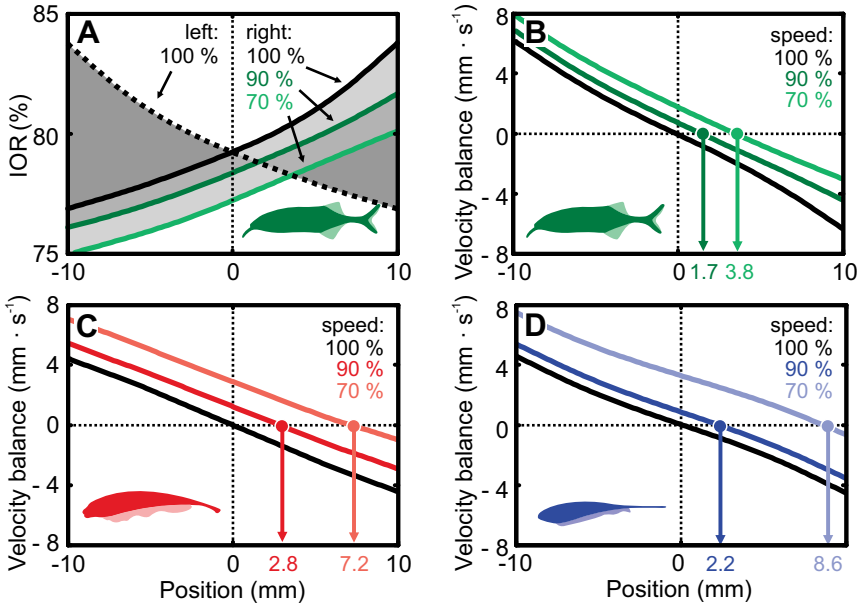

Fig. S4. Prediction of the perceptual center of the shuttle under different speed conditions for the different species. (*A*) IOR curves for BEM data in *Gnathonemus* assuming a rostral–caudal object translation of 8 cm (100% speed condition). Black dotted line shows the IOR for the *Left* side of the shuttle object, and the solid black line shows the data for the *Right* side. For the different speed conditions, the relative translation of the object decreases on one side (dark green, 90% = 7.2 cm; light green, 70% = 5.6 cm). As a result, the characteristics of the IOR curves change and the curves are offset along the *y* axis. (*B*) Velocity balance (difference in *Left* vs. *Right* IOR curves shown in *A*, and scaled to 2 cm·s^{-1}) for control (black line) and parallax speed conditions (dark green, 90%; light green, 70%) for *Gnathonemus*. The location at which the velocity balance curve intercepts the abscissa predicts the perceptual center of the shuttle. Based on the IOR data calculated for *Gnathonemus*, this was shifted 1.7 mm (90%) and 3.8 mm (70%) from the actual center toward the slower side of the shuttle. (*C* and *D*) Same as *B* but for *Apteronotus* (*C*, predicted perceptual center 90%: 2.8 mm; 70%: 7.2 mm) and *Eigenmannia* (*D*, 90%: 2.2 mm; 70% 8.6 mm).

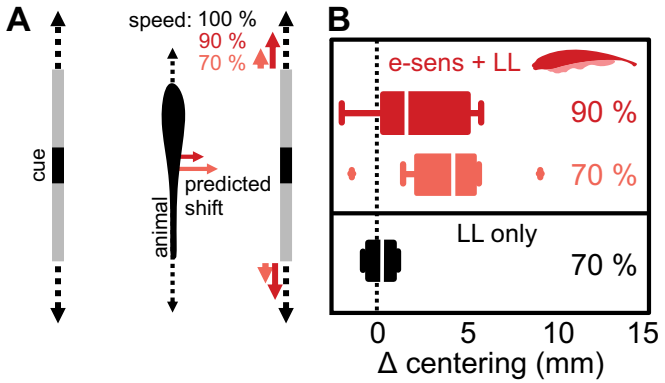

Fig. S5. Hydrodynamic cues do not contribute to distance estimation in our setup. (*A*) *Top* view of the fish between the shuttle walls. The motion of the shuttle walls, and specifically the edges of the shuttle and the slit, will produce water motions which fish can detect and analyze using the mechanosensory lateral line system (1, 2). To determine whether the shuttle walls themselves produce mechanosensory cues, we performed an additional set of experiments using a shuttle without slits, and with and without electrosensory cues. Fish (*Apteronotus*) were tested in the 70% parallax condition (motion of shuttle wall 1.4 $cm{\cdot}s^{-1}$ vs. 2 $cm{\cdot}s^{-1}$) with either a metal-filled slit in the shuttle wall or a solid shuttle wall in addition to the usual control condition. (*B*) The fish consistently shifted their position toward the slower moving side of the shuttle when both mechanosensory lateral line (LL) and electrosensory (metal-filled slit) cues were available ("e-sens + LL": dark and light red; Wilcoxon-signed-rank test: 70%, $n = 9$, $P = 0.01$, data are the same as in Fig. 2*C*). However, with only mechanosensory cues present, the position did not change significantly ("LL only": black; Wilcoxon-signed-rank test: 70%, $n = 4$, $P = 0.62$). This indicates that the mechanosensory cues are not sufficient to mediate the observed behavior (compare Fig. 2*C*).

1. Bleckmann H, Zelick R (2009) Lateral line system of fish. *Integr Zool* 4:13–25.
2. Nelson ME, MacIver MA, Coombs S (2002) Modeling electrosensory and mechanosensory images during the predatory behavior of weakly electric fish. *Brain Behav Evol* 59:199–210.

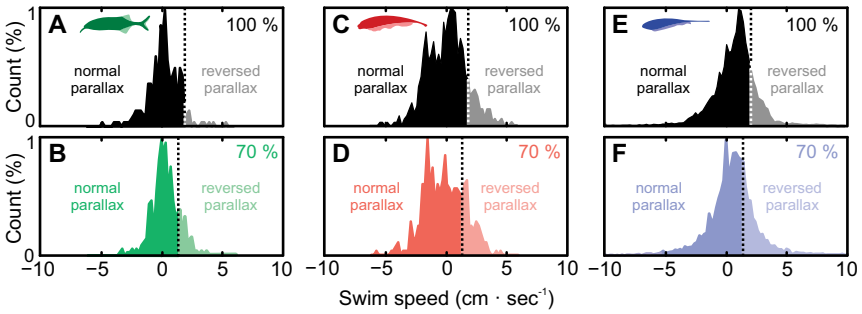

Fig. S6. Swimming speed during centering behavior. Histograms of the swim speed during centering behavior in the three species. (*A*, *C*, and *E*) Control data (both shuttle walls moving at the same speed) for each species (green, *G. petersii*; red, *A. albifrons*; and blue, *E. virescens*). (*B*, *D*, and *F*) Data obtained for the 70% parallax condition. In all panels, positive speeds represent the fish moving in-phase with the shuttle walls and negative values out-of-phase. Vertical dotted lines in all graphs depict the critical speed that is the average speed of the two shuttle walls. Swimming at speeds above this critical speed during parallax trials ("reversed parallax": light shaded regions) potentially leads to contradictory parallax information. For the majority of the data, swim speeds are below this critical value ("normal parallax": dark solid color).

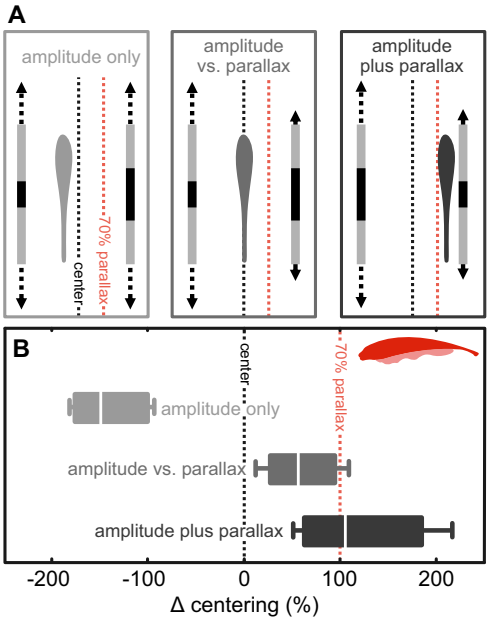

Fig. S7. Static electric image cues contribute to the centering behavior. (*A*) To test the influence of image amplitude comparison between the two shuttle sides, we performed experiments (*Apteronotus*) using various combinations of shuttle motion speeds (slow and fast: 1.4 vs. 2 cm·s^{-1}) and cue sizes (small vs. large: 1 vs. 2 cm metal slit). Specifically, we created experimental conditions in which only amplitude information was available ("amplitude only": light gray, *Left*), amplitude and parallax information were contradictory ("amplitude vs. parallax": intermediate gray, *Middle*), and where both cues provided consistent information ("amplitude plus parallax": dark gray, *Right*). The fish schematic depicts the predicted effects on fish centering behavior. (*B*) Centering behavior for the three test conditions shown in *A*. The shift in fish position from the center of the shuttle (black dotted line) is shown relative to that observed during 70% parallax condition (red dotted line, see also Fig. 2*C*). The behavioral responses were in line with predictions: (*i*) when the amplitude cue was presented without parallax information available (light gray), fish moved away from the shuttle center toward the smaller object (Wilcoxon signed rank test, compared with 70% parallax condition indicated by red dotted line; $n = 6$, $P = 0.03$); (*ii*) when parallax and amplitude cues were in conflict (intermediate gray), fish shifted their position toward the slower moving side (parallax) but the magnitude of the shift was reduced ($n = 6$, $P = 0.03$); and (*iii*) when amplitude and parallax cues were consistent (dark gray), the shift magnitude was similar to those observed for the 70% parallax condition (with the distribution skewed to higher values; $n = 6$, $P = 0.56$).

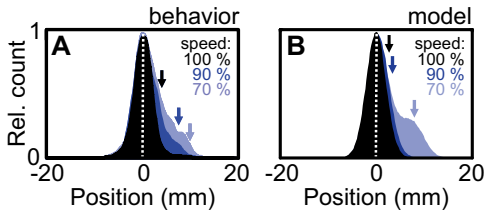

Fig. S8. A stochastic switch between competing sensory cues can explain the shape of the position distributions obtained during behavioral experiments. (*A*) Position distributions obtained during behavioral experiments for *Eigenmannia* (black, control; dark blue, 90% speed; and light blue, 70%, data are the same as in Fig. 2*B*). (*B*) Position distributions obtained from a stochastic behavioral model (see *Supporting Information*; $\beta = 0.3$, $\tau = 1$, $\sigma = 0.25$, and $P = 0.8$). Two competing cues were used as sensory inputs to obtain each position distribution. While one cue was independent of the speed conditions (i.e., amplitude balance cue) the other was dependent on speed conditions (i.e., parallax cue). While the independent cue predicted the shuttle center to be at position 0 in all cases, the prediction of the dependent cue was varied based on the predictions presented in Fig. S4*D* (black, control = 0 mm; dark blue, 90% = 2.2 mm; and light blue, 70% = 8.6 mm). Similar to the experimental data, the position distribution obtained from our model increased gradually in skewness.

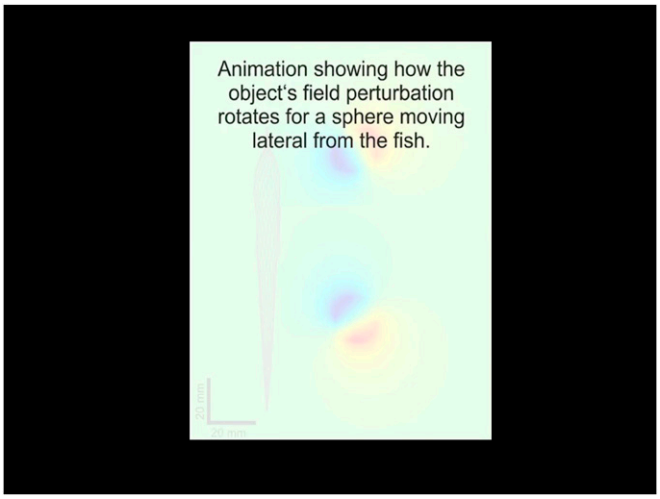

Movie S1. Animation of the distance dependent change of an object's polarization direction. Animation based on the modeled electric field perturbations due to a conductive sphere (2-cm diameter) positioned at different rostral–caudal locations and lateral distances in *Gnathonemus petersii*. The field perturbations show that the gradient of the polarization is oriented along the electric field lines (Fig. 1*A*). The rotation of the polarization gradient is quantified by the angle α, which systematically rotates in a clockwise manner as the object is approaching the animal from a caudal position in the electric field (Fig. S1). The animation then shows identical data for the same object approaching and receding at a rostral position. Contrary to the approach in the caudal field, the polarization gradient now rotates in a counterclockwise manner. The difference of the polarization angle relative to the fish's rostro–caudal axis between the rostral and caudal object positions are then plotted ($\Delta\alpha$). This decreases linearly with decreasing lateral distance and can serve as a parallax-like electrosensory cue where different apparent speeds of EI movements will occur for rostrocaudal sweep motions carried out at different lateral distances (Movie S2).

Movie S1

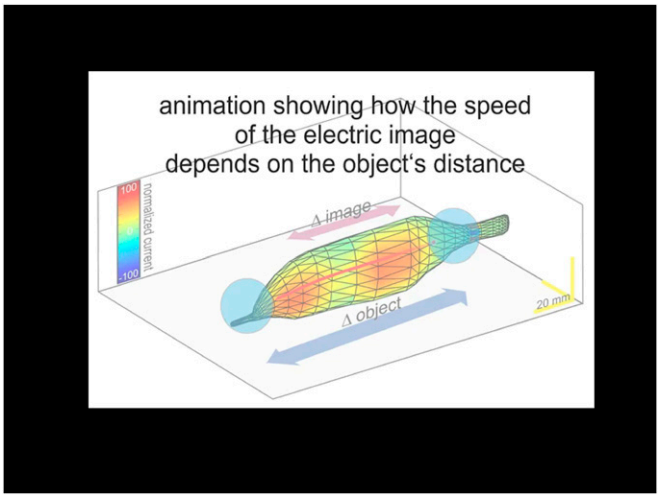

Movie S2. Animation of the effect of lateral distance on the apparent speed of the electric image on the sensory surface (IOR). Animation showing the functional consequence of the distance- and position-dependent polarization gradient. Here, we show the modeled normalized electric images of a conductive sphere (1-cm radius) for the sphere sweeping along the side of *Gnathonemus petersii* at a fixed lateral distance (first sweep, 24 mm distance and second sweep, 13 mm). Whereas the range of the object's movement is fixed (Δ object), the range by which the electric image moves over the fish's skin (Δ image) decreases with lateral distance. This results in a distance-dependent image–object ratio (IOR = $\Delta_{image}/\Delta_{object}$), indicating that the apparent speed of EI motion depends on distance to the object and might serve as a distance estimation cue.

Movie S2